SAND2023-07963C

An investigation into the effects of state of charge and heating rate on propagating thermal runaway in Li-ion batteries with experiments and simulations

Andrew Kurzawski[a*], Lucas Gray[b], Loraine Torres-Castro[c], John Hewson[d]

[a]Sandia National Laboratories, P. O. Box 5800, Albuquerque, NM 87185-1135, USA, akurzaw@sandia.gov

[b]Sandia National Laboratories, P. O. Box 5800, Albuquerque, NM 87185-1135, USA, lgray@sandia.gov

[c]Sandia National Laboratories, P. O. Box 5800, Albuquerque, NM 87185-1135, USA, ltorre@sandia.gov

[d]Sandia National Laboratories, P. O. Box 5800, Albuquerque, NM 87185-1135, USA, jchewso@sandia.gov

*Corresponding author

Highlights:

- Understanding propagating thermal runaway is critical to safer battery system design.
- Experiments were conducted on packs of three Li-ion cells with different heating rates and states of charge.
- Decreasing state of charge slows down propagation, while a slower heating rate increases propagation speed.
- Simulations were conducted with a new diffusion-limited reaction model and generally agree with experiments on propagation timings.

Abstract:

As large systems of Li-ion batteries are being increasingly deployed, the safety of such systems must be assessed. Due to the high cost of testing large systems, it is important to extract key safety information from any available experiments. Developing validated predictive models that can be exercised at larger scales offers an opportunity to augment experimental data. In this work, experiments were conducted on packs of three Li-ion pouch cells with different heating rates and states of charge (SOC) to assess the propagation behavior of a module undergoing thermal runaway. The variable heating rates represent slow or fast heating that a module may experience in a system. As the SOC decreases, propagation slows down and eventually becomes mitigated. It was found that the SOC boundary between propagation and mitigation was higher at a heating rate of 50^{o}C/min than at 10^{o}C/min for these cells. However, due to increased pre-heating at the lower heating rate, the propagation speed increased. Simulations were conducted with a new intra-particle diffusion-limited reaction model for a range of anode particle sizes. Propagation speeds and onset times were generally well predicted, and the variability in the

Sandia National Laboratories is a multimission laboratory managed and operated by National Technology & Engineering Solutions of Sandia, LLC, a wholly owned subsidiary of Honeywell International Inc., for the U.S. Department of Energy's National Nuclear Security Administration under contract DE-NA0003525.

propagation/mitigation boundary highlighted the need for greater uncertainty quantification of the predictions.

Keywords: Li-ion batteries, thermal runaway, energy storage safety

1 Introduction

The prevalence of lithium-ion batteries and risks associated with thermal runaway necessitates a thorough understanding of battery failures. While the likelihood of a single cell failing and going into thermal runaway is low, as systems of batteries become larger, the impact of a single cell failure propagating to adjacent cells and materials increases. The resulting fire and flammable gases threaten the safety of nearby people and first responders and could result in extensive property damage if not mitigated.

The speed at which thermal runaway propagates through a system of cells is critical to make decisions related to system safety. In the context of stationary energy storage systems (ESS), the propagation time is important for determining how quickly fire prevention intervention actions must be conducted, while in the context of electric vehicles (EV), passenger egress time is of importance. If there are sufficient active interventions or passive mitigation measures in the system, the speed at which thermal runaway propagates can be decreased or even mitigated entirely.

Many factors influence the thermal runaway behavior including the cell chemistry and form-factor, system design and materials, and current operating conditions such as temperature and state of charge (SOC) [1]. Each of these factors affect how easily a cell goes into thermal runaway. The boundary between propagation and mitigation is the result of a competition between the chemical heat-release rate (HRR) from thermal runaway and the heat dissipation rate through a variety of paths; the outcome of this competition determines if propagation will be sustained. While larger cells release more energy, and different cell chemistries have a range of energy densities, the SOC has a large impact on the HRR. As the SOC increases, more energy is released during thermal runaway and at higher rates [2, 3, 4].

To slow down or mitigate propagating thermal runaway at the "module scale", one must either decrease the available energy or increase heat dissipation. Investigations of heat dissipation have been conducted with the surrounding fluid (e.g. forced air cooling or water mist) [5] and with inert materials (e.g. casing or structural supports) [6, 7]. Here, increasing the heat transfer rate or heat capacity decreases the heating rate of adjacent cells. To decrease the available energy, a lower energy density cell can be used or the SOC can be reduced.

A range of research has been conducted on propagating thermal runaway versus SOC at the module-scale. Torres-Castro et al. [6] looked at SOCs between 50% and 100% and found that mitigation occurred between 75% and 80% SOC for thermal runaway initiated with nail penetration. For these same cells and configuration, adding thermal masses to reduce the energy density led to mitigation at a similar energy density as observed for the SOC [6, 8]. Huang et al. investigated the effects of SOC and heating rate on thermal runaway in large-format prismatic cells [9]. They found that thermal runaway in single cells is faster and releases more energy with

increasing SOC, while lowering the heating rate increases cell preheating and speeds up propagation across the cell. Lee et al. [10] tested arrangements of cylindrical cells between 50% and 100% SOC. Propagation times were measured, and cells at 50% SOC were observed to propagate 8.5 times slower through the arrangement and release less energy than 100% SOC. Fang et al. examined the effect of spacing and SOC for vertically stacked cylindrical cells and found mitigation occurred at 50% SOC for this configuration [11].

At the system scale, limited thermal runaway data is publicly available and the impact of factors such as SOC or arrangement of casing/supporting materials is not well understood. Ditch and Zeng [12] offer some insights into the scale-up from module to ESS "rack scale" for two different cell chemistries. In the rack scale scenario, there can be fast or slow heating of modules depending on the nearby fire environment and other modules. There is a need to understand how the rate of pre-heating affects the HRR characteristics at the module scale, as this feeds into the propagation time and window of opportunity for suppression or mitigation. Jin et al. [13] studied thermal runaway propagation for a range of external heating rates both experimentally and computationally in the context of determining a minimally invasive initiation source. They reported faster initiation times at higher heater powers and faster propagation rates with increased pre-heating.

In this work we examine a scenario where two characteristic heating rates are applied to a small "module" consisting of three pouch cells at a range of SOCs to evaluate propagation behavior. This scenario represents heating of a module from an external source such as flame impingement on the external case or soaking in hot gases. The presence of a module case acts as a thermal buffer between the cells and environment, so peak heat fluxes will be lower than direct flame impingement on the cells. These initiation scenarios are not typically studied in literature. Here we demonstrate how preheating rate will change the initiation and propagation behavior of thermal runaway. These experiments seek to augment findings from literature by identifying differences in the SOC at the boundary between thermal runaway propagation and mitigation due to different preheating (via two heating rates). Simulations using the software LIM1TR (Lithium-Ion Modeling with 1-D Thermal Runaway) are tested against these scenarios [14]. This work also demonstrates that the boundary can be predicted through the use of recent models [8], and the effects of uncertain model parameters are discussed.

2 Methods

To explore thermal runaway behavior at a range of SOCs and external heating conditions, heater-induced thermal runaway and propagation was measured in three pouch-cell stacks sandwiched between brass blocks held in place by long screws. This section details the experimental apparatus, test matrix, and simulation methods used to study this scenario.

2.1 Experimental conditions

A side view diagram and picture of the system are shown in Figure 1. The pouch cells have a capacity of 4 Ah and lithium cobalt oxide (LCO) cathode material with graphite anodes. The pouch dimensions are 7 mm by 46 mm by 138 mm, and the cells weigh 90 g. The heater is constructed from two 1000 W cylindrical cartridge heaters embedded in a brass block with

dimensions 19.05 mm by 76.2 mm by 146.05 mm. From left to right, the experimental stack is composed of the brass heater block, a single layer of Kapton tape, three pouch cells, a phenolic resin backing block (12.7 mm by 76.2 mm by 146.05 mm), and a solid brass block with the same external dimensions as the heater block. This stack is held in place by four threaded rods running through the corners of the brass blocks.

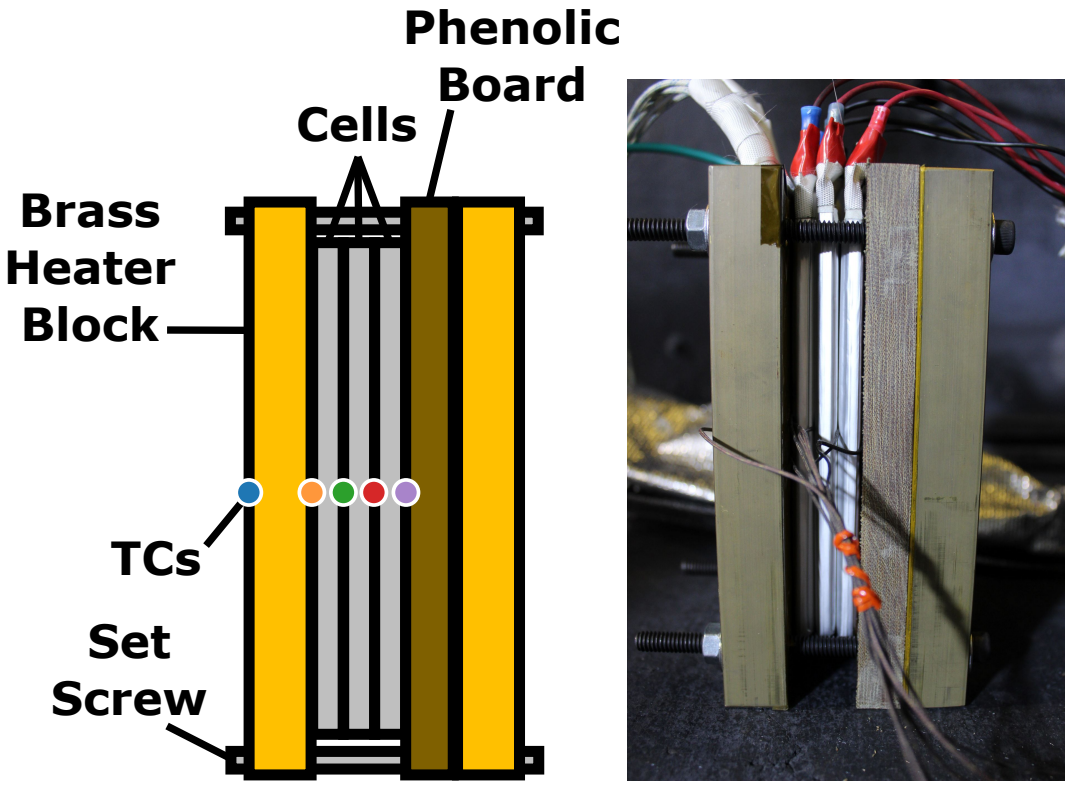

Figure 1: Illustration with labeled components (left) and picture (right) of the experimental setup.

Temperature measurements were collected with Type-K thermocouples (TCs) located along the centerline of the stack. Going from left to right in Figure 1, the first TC is located on the outside of the heater, and the second TC is between the Kapton tape and cell 1. The next two TCs are between cells 1 and 2, and cells 2 and 3. The final TC is between cell 3 and the phenolic board. In order, these TCs are abbreviated H, H-C1, C1-C2, C2-C3, and C3-P to denote their position within the stack. The cells are not electrically connected, and the voltages of each cell were collected as another indicator of failure. Ambient temperature was between 21^{o}C and 23.5^{o}C for all experiments.

Two heating rates were chosen for this experimental campaign to capture different pre-heating scenarios, namely 10^{o}C/min and 50^{o}C/min. The heating rate of the heater cartridges was controlled with an Automation Direct SOLO 9696 temperature controller based on an additional TC placed between the cell and the heater block in the center of the cell. The heaters were turned off at either 300^{o}C or once thermal runaway was observed. This scenario focus on heating from the side of a module, but one could imagine scenarios where the entire module is soaking in hot gas providing even heating or there is minimal module casing and cells are directly exposed to venting from adjacent modules. For a large multi-cell module heated from the side, cells farther

from the heat source would encounter minimal preheating and propagation behavior would be similar to propagation from cell 2 to 3 at the high heating rate in the present experiments.

The heating rates of 10°C/min and 50°C/min correspond to initiation of thermal runaway after approximately 20 minutes and 5 minutes, respectively. While limited system-scale thermal runaway data is available in the literature, Ditch and Zeng [12] report module temperature and heat-release rate data for system-scale experiments where thermal runaway was initiated in a module. The authors collect the time after flaming ignition of the first module when all other modules exceed a threshold temperature as an indicator of module-to-module propagation times. The time for a second module to initiate was on the order of 10 to 20 minutes, and the 10°C/min heating rate was chosen to reflect the first propagation event (i.e. from the initiating module to the second module to go into thermal runaway). Once the second module began thermal runaway, other modules typically followed within 5 minutes as the fire cascaded through the system. The 50°C/min heating rate represents this faster spread through a system after multiple modules have become involved.

The full cell-to-cell propagation test matrix is shown in Table 1 with repeated measurements marked with asterisks. Both heating rates were applied to cells at 25%, 50%, 75%, and 100% SOC. The additional SOCs were chosen sequentially to search for the boundary between propagation and mitigation within 5% SOC. The propagation versus mitigation behavior is listed in Table 1 to show the SOC selection, and details of the propagation behavior will be discussed in Section 3.1.

Table 1: Experimental matrix and propagation status (*denotes SOCs with replicas).

Heating Rate	10°C/min					50°C/min					
SOC (%)	20	25	50	75	100	25	35*	40*	50	75	100
Propagation (Y/N)	N	Y	Y	Y	Y	N	N	Y/N	Y	Y	Y

2.2 Computational model

The computational tool LIM1TR was used in this work to model heat transfer and reaction kinetics of thermal runaway [14]. This software is targeted at simulating stacks of cells as a quasi-1D domain, since the thermal conductivity in the plane of the electrodes is much greater than the thermal conductivity parallel to the electrodes. The cells and inert materials are then "lumped" in the parallel directions (Biot number approximately 0.007) and the transient heat equation is solved in the perpendicular direction with heat losses to the surroundings around the perimeter of the stack. This quasi-1D formulation decreases computational time at the expense of accuracy, with inaccuracy proportional to the inverse stack Biot number. This system is discretized in space using the finite volume method with temporal integration provided by Spitfire [15].

A thermal contact resistance of 0.004 m^2K/W is applied between each of the layers based on Torres-Castro et al. [6]. Additional uncertainty exists in the thermal contact resistance between the heater and cell 1 due to the difference in materials, but for the purposes of this investigation the layer of Kapton tape is assumed to have similar contact properties to the pouch material.

Heat losses are modeled at all external surfaces with an effective heat transfer coefficient representing convective and linearized radiative contributions. This heat transfer coefficient is 10 W/m^2/K for all surfaces except the left face of the heater block. In lieu of a heater power control algorithm, the left heater boundary is modeled as a constant temperature ramp rate during heater operation and effective heat transfer coefficient of 15 W/m^2/K after the heater is turned off. Heat transfer from the vented gases is not considered in this work as the cells are not directly exposed to venting jets, and the contact surface area between cells is larger than the exposed surface area, resulting in conduction dominated heat transfer.

As the heater controller in the experimental system tracks the TC between the heater and cell 1, prescribing the left side temperature ramp rate in ^{o}C/min required an inversion process. Using the RMSE error for the predicted and measured temperatures at the H-C1 thermocouple for the first 1000 seconds and 200 seconds of the 10^{o}C/min and 50^{o}C/min experiments, respectively, numerical simulations were conducted with LIM1TR to invert for the effective temperature ramp rate on the left boundary. These rates are higher than the prescribed heating rates due to the thermal mass of the brass heater and heat losses out the sides.

A full tear-down of the cells was not conducted so there is uncertainty in the mass fractions of the electrodes, current collectors, casing, etc. Torres-Castro conducted propagation experiments on smaller 3 Ah pouch cells and the mass fraction breakdown is assumed to be constant between 3 Ah and 4 Ah LCO pouch cells [6], and the initial mass concentrations in this work are calculated with these fractions and the weight of the 4 Ah cells (90 g).

The energy release from thermal runaway is predicted by a system of three reactions described in Kurzawski et al. [8]. In summary, the model includes solid-electrolyte interphase (SEI) decomposition, an anode-electrolyte reaction, and a cathode-electrolyte reaction. Further details on the individual reactions can be found in [8, 16, 17, 18]. Kurzawski et al. theorize that intra-particle mass transport becomes limiting at higher temperatures and developed a modified source term to serially combine the electrode-electrolyte reactions with the solid-state diffusion rate through an idealized spherical shell representing the electrode particles. Figure 2 depicts a spherical particle described by an outer radius, r_o, where the reacting species diffuses through a shell from an inner radius, r_i, to the surface of the particle. The modified reaction rate takes the form

$$k'_j = \frac{k_j}{1 + Da_j}, \tag{1}$$

for electrode j, where k_j is the reaction rate constant. A Damköhler number for the ratio of the chemical reaction rate to diffusion through the spherical shell is given as

$$Da_j = \frac{A_j exp(-E_j/RT)(r_{o,j} - r_{i,j})}{a_p \rho D_{0,j} exp(-E_{D,j}/RT)} \frac{r_{o,j}}{r_{i,j}}. \tag{2}$$

The Damköhler number is a function of the reaction rate with a pre-exponential factor, A_j, activation energy, E_j. In the denominator, the diffusion coefficient $D_{0,j} exp(-E_{D,j}/RT)$ with the specific particle area, a_p, and material density, ρ, reduces the effective activation energy and becomes limiting at high temperatures. Values for the diffusion pre-exponential factor and activation energy ($D_{0,j}$ and $E_{D,j}$, respectively) are given in Ref. [19].

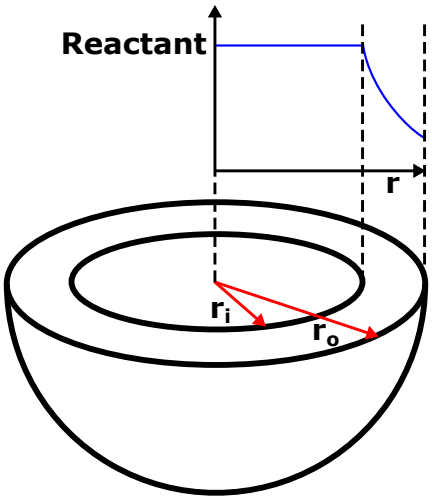

Figure 2: Idealized electrode particle with reactant transport through a spherical shell.

In past work the inner radius was fixed at a constant value [8], but here the inner radius varies with reactant concentration, ρ_s relative to initial concentration is $\rho_{s,o}$, representing transient diffusion-limited reactant depletion. For species s, the inner radius is

$$r_{i,j} = r_{o,j} \left(\frac{\rho_s}{\rho_{s,o}} \right)^{1/3}. \tag{3}$$

The reacting species are LiC_6 and CoO_2 for the anode and cathode, respectively. This expression for the inner radius is then substituted into Equation 2 and solved in LIM1TR.

In thermal runaway predictions, the anode-electrolyte reaction accelerates more gradually with temperature, so the cathode-electrolyte reaction runs to completion first. The anode is then left to complete the heat release if sufficient heat had been generated by the cathode reaction to sustain thermal runaway [8]. Since propagation is more sensitive to the highest temperature reaction rates, the anode-electrolyte source term has greater sensitivity and will be the focus of a parameter study in Section 3.2.

The Brunauer-Emmett-Teller (BET) surface area is an important input for the Shurtz anode reaction model [16, 17], and it will be varied as a function of particle size in this work. Baseline simulations were conducted with the particle radii from Guo et al. [19] for an LCO cathode and graphite anode of 8.6 μm and 12.5 μm, respectively, and an anode BET surface area of 1.1 m^2/g as in the original model [8].

In the diffusion limited reaction, larger particles will have a greater effect on limiting the reaction rate as the reacting species are depleted. Zaghib et al. [20] report the relation between graphite particle size and BET surface area for a range of graphite particle sizes. Simulations with different anode particle sizes and corresponding surface areas will be encoded as R6, R10, etc., where the number after "R" is the particle radius in micrometers. We note that Shurtz [17] provides a correlation for the specific particle edge area and BET surface area which will be used for a_p.

We understand that without knowledge of the cell composition and construction from the manufacturer or a full tear-down of a cell, there is uncertainty associated with several of the

simulation inputs such as component mass fractions, electrolyte composition, electrode characteristics, etc. Therefore, it is possible that a different set of parameters could produce better thermal runaway predictions. This argument could also be made for the chosen reaction models. We operate under the assumption that these models capture the leading order physics based on comparisons to calorimetry and propagation experiments from the literature.

3 Results

3.1 Experimental results

Experiments were run for each heating rate at a range of SOCs to examine the propagation behavior: the time at which the first cell fails, the speed at which propagation occurs, the boundary between propagation and mitigation, and the heat released during thermal runaway. The 100% SOC temperatures and voltages for both heating rates, shown in Figure 3, follow the expected behavior of pouch cell propagation as seen throughout the literature [6, 7, 21, 9]. Following the failure of cell 1, thermal runaway propagates through cells 2 and 3 in approximately 30 seconds for both cases. Failure of the cells is indicated by a loss of voltage and/or rapid rise in temperature, and the implications of these two markers will be discussed at the end of this section.

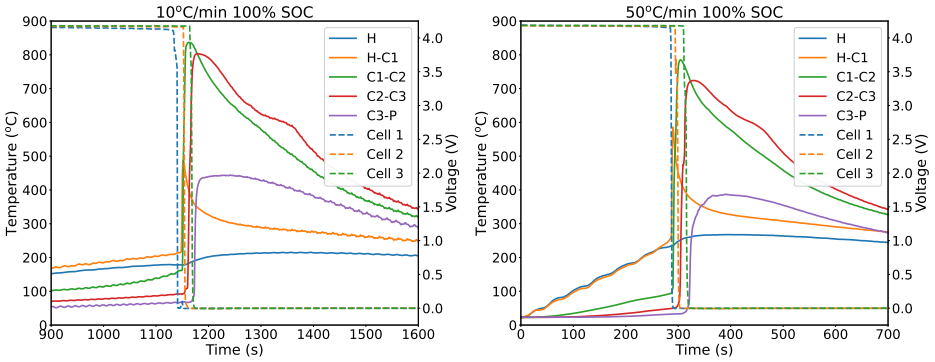

Figure 3: 100% SOC temperatures (solid lines) and voltages (dashed lines) for 10°C/min (left) and 50°C/min (right).

Mitigation of thermal runaway occurred between 20%-25% SOC for the 10°C/min heating rate and 35%-40% SOC for the 50°C/min heating rate. Thermal runaway occurs when the cell reaches a temperature where heat release can accelerate. Slower heating allows more heat to spread through the cell stack before the heater-side temperature reaches this thermal-runaway temperature, leading to greater preheating of the entire cell stack and lowering the SOC where mitigation occurred. Figure 4 shows the SOCs on either side of the propagation/mitigation boundary. In the 20% SOC case, cell 2 is seen to fail through loss of voltage and an associated weak heat release seen between 1600 and 1800 seconds in the TCs on either side of cell 2 (C1-C2 and C2-C3). At 25% SOC, this weak energy generation carries on slowly through the stack, where cell 3 loses voltage 569 seconds after cell 1.

The boundary between propagation and mitigation is less clear at the 50°C/min heating rate. Temperatures and voltages from 35% SOC and 40% SOC are shown in Figure 5. Both replicates of 35% SOC failed to fully propagate with cell 1 failing and a mild heat release observed when

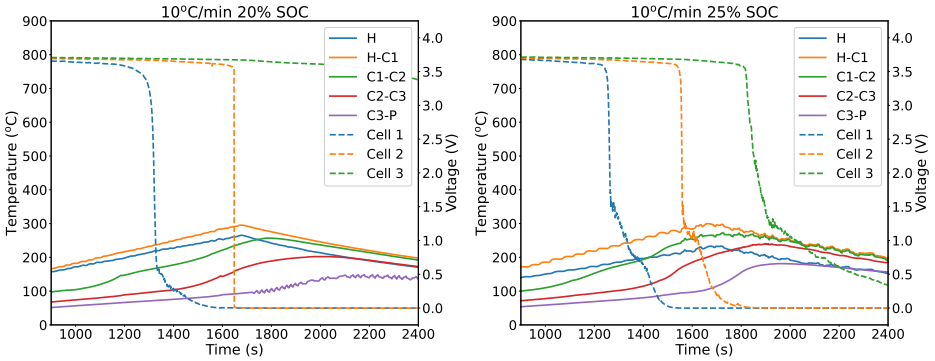

Figure 4: Mitigating SOC boundary temperatures (solid lines) and voltages (dashed lines) for 20% SOC (left) and 25% SOC (right) at 10°C/min.

cell 2 failed between 500 and 600 seconds. These cases are considered to be "mitigated" as there was insufficient energy generated from thermal runaway to sustain cascading failure.

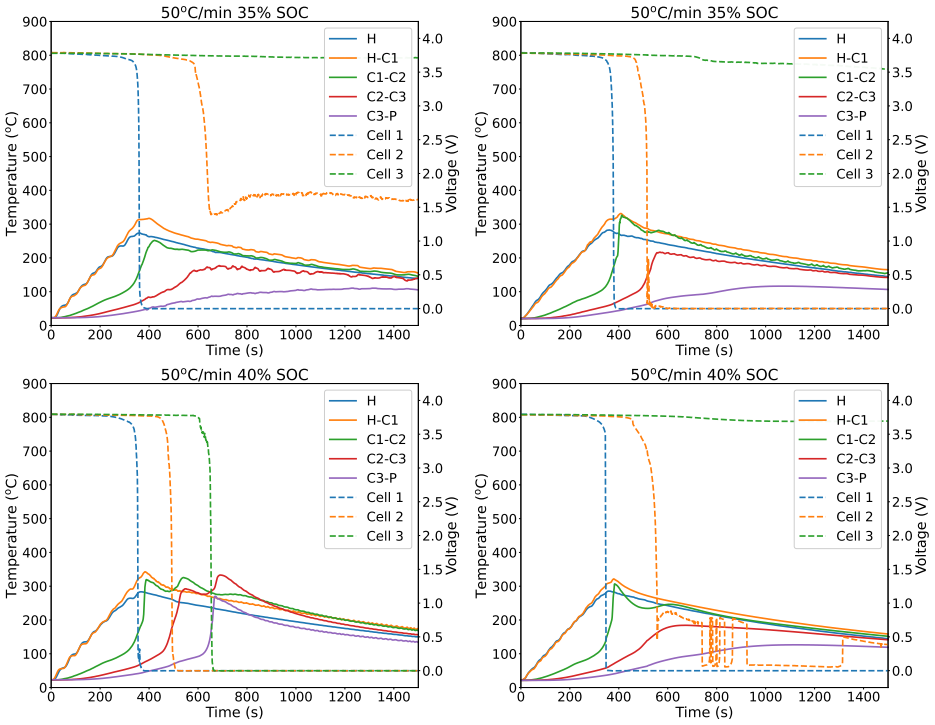

Figure 5: Temperatures (solid lines) and voltages (dashed lines) of borderline propagation cases at 50°C/min: 35% SOC replicates (top) and 40% SOC replicates (bottom left and bottom right).

At 40% SOC, one replicate weakly propagated over the course of around 5 minutes (Fig. 5 bottom left) while thermal runaway was mitigated between cells 2 and 3 in the other replicate (Fig. 5 bottom right). Thermal runaway needs only for energy generation to exceed dissipation for the reaction to become fast and "run away", and a variety of parameters can affect this balance including local differences in thermal contact resistance and cell-to-cell manufacturing variations among others. These contribute to the overall uncertainty in the propagation/mitigation boundary,

and in lieu of a statistically significant number of replicates these data simply show that the boundary is near 40% SOC. A much stronger thermal runaway response is observed at 50% SOC with temperature rise from self-heating in excess of 50°C, indicating the propagation/mitigation boundary is below 50% SOC.

A summary of the peak thermocouple temperatures for both heating rates is shown in Figure 6. Peak temperatures decrease with SOC as less active material is available in the cells to fuel thermal runaway, and a more precipitous change in peak temperatures occurs close to the propagation/mitigation boundary. For all cases, the outside heater temperature, 'H', remains relatively constant as the heater is thermally large relative to the cells and dampens the thermal wave from cell 1. Even from this small sample size, test-to-test variations of around 50°C are observed in the 35% SOC replicates. These differences between peak temperatures are indicative of local variability in thermal runaway and sensor measurements, as this process can be dynamic with internal pressures, gas and particulate transport, and venting. While the system is constrained with set screws, changes in thermal contact during this process are expected to have an effect on TC readings.

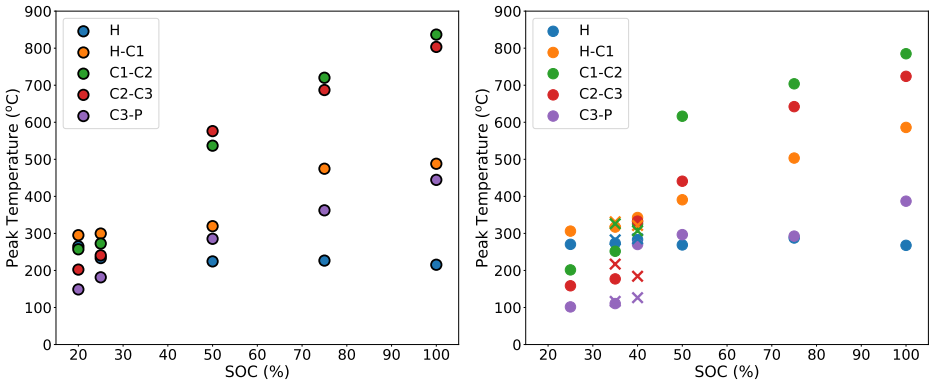

Figure 6: Peak temperature for 10°C/min (left) and 50°C/min with replicates indicated by the 'X' symbol (right).

The cell voltage can be used to understand the speed at which thermal runaway propagates through a module of cells. The time that the voltage of each cell dropped below 90% of the initial value is shown in Figure 7 (left). In general, as the SOC increases above 50%, cell 1 fails sooner and the delay between cell 1 and cell 3 is shorter. For some cases that did not propagate, cell 3 lost voltage at later times not shown in this plot while no thermal signature was observed.

To get a more complete picture of the propagation speed, the voltage drop and TC measurements must be examined together. Using the method from Torres-Castro et al. [6], TC measurements were post-processed to get the peak heat release times of the cells. TCs between cells that propagate will see two distinct peaks in the temperature rate (i.e. a rapid increase in temperature): the first when the thermal runaway front arrives from the cell that has already failed and the second peak when the next cell begins thermal runaway. TCs between cells and inert materials or non-propagating cells will typically see a single fast rise in temperature.

Figure 7 (right) collates the voltage and temperature-based propagation times at SOCs of 50% and greater for both heating rates. The voltage-based propagation time is the difference between

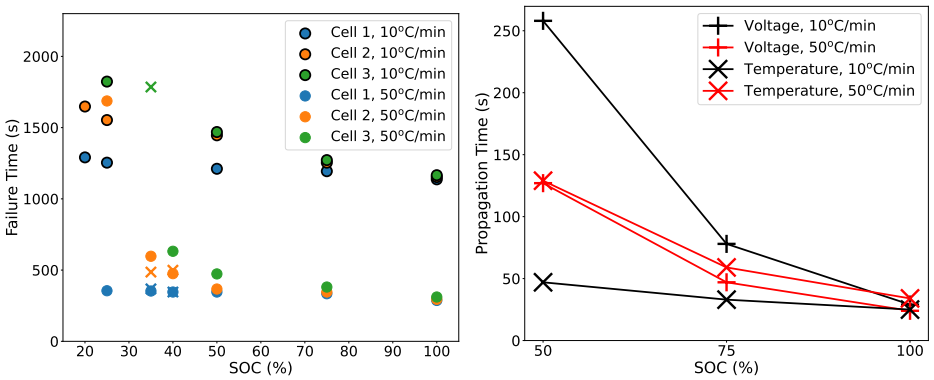

Figure 7: Cell failure times based on voltage drop for both heating rates with replicates indicated by the 'X' symbol (left) and thermal runaway propagation times based on voltage drop and temperature rise for both heating rates (right).

cell 1 and cell 3 losing voltage. The temperature-based time is the difference between the peaks at TCs 'H-C1' and 'C3-P' signifying the beginning of thermal runaway in cell 1 and the completion of thermal runaway in cell 3. We note that below 50% SOC, the heat release rate was too slow to capture distinct peaks in the temperature measurements.

At 100% SOC, propagation times are similar for both heating rates and both timing methods, between 24 and 34 seconds. At all other SOCs with the low heating rate (black symbols), the voltage-based times (+ symbols) are consistently longer than the thermal times (X symbols). Examination of the data shows that the voltage in cell 1 dropped with a small temperature rise, followed by a delay before fast thermal runaway began, and this delay is longer at lower SOCs. Voltage loss before full thermal runaway could be due to separator failure and/or gas generation from SEI decomposition. This indicates that voltage loss may not be a good indicator for thermal runaway propagation speed for slow heating rates, corroborating the findings of Archibald et al. [21].

For the higher heating rate (red symbols), differences in the timing methods are smaller with the temperature-based time being longer. This is because cell 3 typically loses voltage at the onset of thermal runaway, while it takes the propagation front on the order of 10 seconds to reach the TC between cell 3 and the phenolic board.

Using the temperature-based propagation time, it is seen that the low heating rate cases propagate faster than the high heating rate cases. This is due to greater pre-heating of cells 2 and 3 before thermal runaway begins in the 10°C/min cases which reduces the amount of heat required to maintain propagation. The implication for the system-scale is that a module soaking in a slow heating environment will propagate faster once thermal runaway begins than a module that is heated quickly from on side.

3.2 Numerical results

Simulations were conducted with LIM1TR to assess predictions of the temperature evolution during thermal runaway and relevant propagation times using the thermochemical model from

Ref. [8] but with the variable radius Damköhler limiter developed in the current work (Eq. 2). Because particle sizes have not been measured for these cells, the sensitivity to a range of particle sizes and BET surface areas is examined in a summary form at the end of this section. The majority of simulations are conducted assuming 15 μm particles (R15) with the BET surface area based on the correlation identified in Sec. 2.2 [20]. Of interest are how well the model captures initiation of thermal runaway in cell 1, how fast thermal runaway propagates through the cells following initiation, and if the simulation predicts the boundary between propagation and mitigation for different levels of pre-heating of the module.

Figure 8 shows comparisons of experiments and simulations for the 50°C/min heating rate at 100% SOC, 50% SOC and 40% SOC for particle size R15. Note that time axes in Figure 8 are shorter at higher SOCs to capture the faster propagation. At 100% SOC these simulations are about 10 seconds faster and initiate a few seconds later than the experiments. At 50% SOC the propagation and heat release are significantly slower. Using the baseline diameter and BET area model from [16, 17] leads to significantly slower initiation at low SOC due to a small BET surface area initially recommended. This slower initiation was noted earlier using a fixed inner radius for the Damköhler limiter [8]. The concentration-dependent inner radius Damköhler limiter form used in this work improves these predictions somewhat. Measurements at 50°C/min heating rate and 40% SOC were identified in Fig. 5 as the propagation/mitigation boundary with one measurement propagating (top right) and a replicate failing to propagate (bottom right). Predictions in Fig. 8 show weak heat release in the first cell and no propagation, showing the boundary between propagation and mitigation is well predicted, but slightly non-conservative, at this heating rate. Peak temperatures at the inter-cell interfaces (C1-C2 and C2-C3) are generally well predicted. These simulations use the R15 particle size model; the variation in the propagation time as a function of the particle size is quantified below.

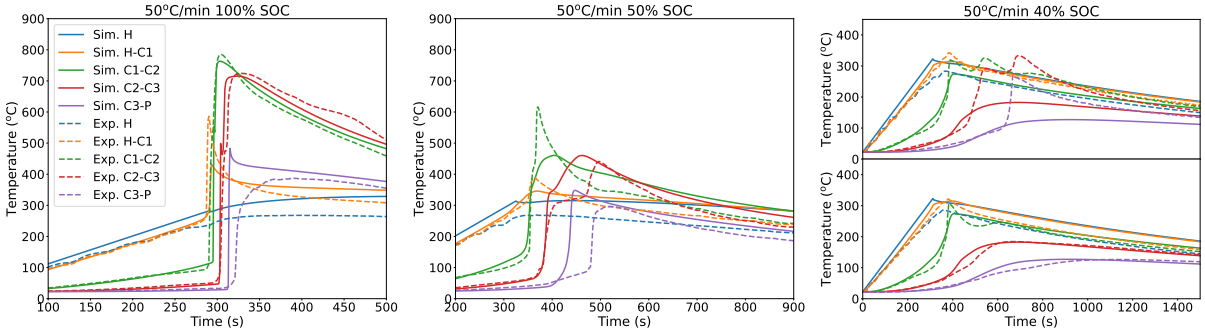

Figure 8: 50°C/min at 100% SOC (left), 50% SOC (center), and both 40% SOC experiments (right) for particle R15. Note solid lines are simulations and dashed lines are experiments.

At the slower 10°C/min heating rate the initiation time is around four times later compared to the 50°C/min heating rate. This allows more heat to spread from the heated cell to subsequent cells 2 and 3. To quantify this preheating we identify the approximate energy added to each of the cells at the time when the first cell in the 100% SOC case experiences thermal runaway. The onset time of cell 1 is identified from simulations as the time when the heating rate of the average cell temperature becomes fast. The energy added is identified from simulations of the 50% SOC case that has not experienced significant chemical heating at this time. The average simulated

temperature rise associated with the energy added by pre-heating is listed in Table 2.

Table 2: Average simulated cell temperature increase prior to thermal runaway.

Heating Rate	Cell 1	Cell 2	Cell 3
10°C/min	156°C	92°C	50°C
50°C/min	151°C	45°C	11°C

While the average temperature of cell 1 is similar between the two heating rates, the slower 10°C/min heating rate has allowed more energy to reach cells 2 and 3. A critical energy must be provided to initiate thermal runaway, and in propagating thermal runaway, this energy is supplied by external pre-heating and thermal runaway in the adjacent cell. In the case of cell 2, approximately twice as much energy has been deposited by preheating with the slower heating rate before cell 1 begins thermal runaway. With thermal runaway initiating at temperatures in the vicinity of 230 °C for these cases, this average temperature rise prior to thermal runaway reduced the required heating to continue propagation. As the heat release is proportional to SOC, propagation is observed at a lower SOC for the lower heating rate. We do note that the five times slower heating rate does not ignite five times later because thermal runaway depends mildly on the temperature gradient as predicted by the Frank-Kamentskii model of inhomogeneous ignition [22].

Figure 9 shows comparisons of experiments and simulations for the slower 10°C/min heating rate at 100% SOC, 50% SOC and 25% SOC. At 100% SOC the initial thermal runaway is slightly delayed relative to measurements, but the overall propagation rate is reasonably well predicted. Thermal runaway predictions at 50% SOC are earlier than measured, and this difference between the 100% and 50% SOC results might be indicative of the uncertainties and stochastic variability in the measurements. At 25% SOC, evidence of heat release is observed in the experiments between 1400 and 1800 seconds. In the simulation, the active material in the anode and cathode of the first cell is completely reacted, but over a longer time scale from 1000 to 2000 seconds, which allows more time for heat dissipation.

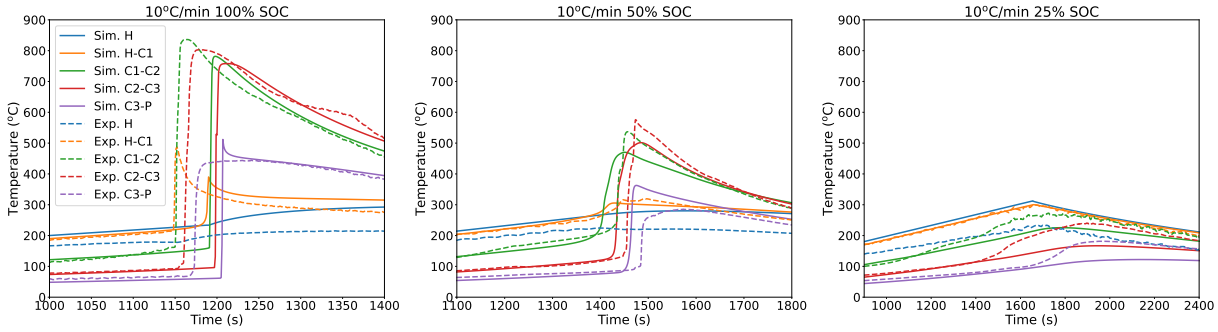

Figure 9: 10°C/min at 100% SOC (left), 50% SOC (center), and 25% SOC (right) for particle R15. Note solid lines are simulations and dashed lines are experiments.

For each of these simulations temperature predictions are somewhat lower than measured and are slightly non-conservative similar to the 50°C/min simulations. It is likely that some relevant physics is not captured in the present model. Relatively little data is available for these conditions

to develop and test these models. To the best of the authors knowledge, this is the first measurement and analysis addressing slower heating rates with cell preheating.

As mentioned above, the particle diameter and BET surface area both appear in the current model but have not been measured. To assess the sensitivity of predictions to these quantities, a range of particle radii (6, 10, 15 and 20 μm) were simulated with BET surface areas for each particle radius determined using the correlation [20]; these are denoted R6, R10, R15 and R20, respectively. Simulations were also conducted with the particle sizes from Guo et al. [19] and a BET surface area of 1.1 m^2/g as in the original model [16, 17, 8] and identified as the base model. For both heating rates, there is no change in the boundary between propagation and mitigation for this range of particle sizes. However, the rate of propagation does vary with the particle size as quantified in Fig. 10. We note that propagation times are computed based on the heating rate method from Section 3.1. Smaller particle sizes with larger surface to volume ratios and shorter diffusion lengths propagate faster, but for this factor of 6.7 change in the particle diameter, the change in the propagation rate is less than a factor of two. Interestingly, the "base" model previously reported with a smaller BET surface area relative to the others propagates substantially slower at 50% SOC. It is recommended that consistency between BET surface area and particle size be maintained in future simulations. These trends hold for both heating rates.

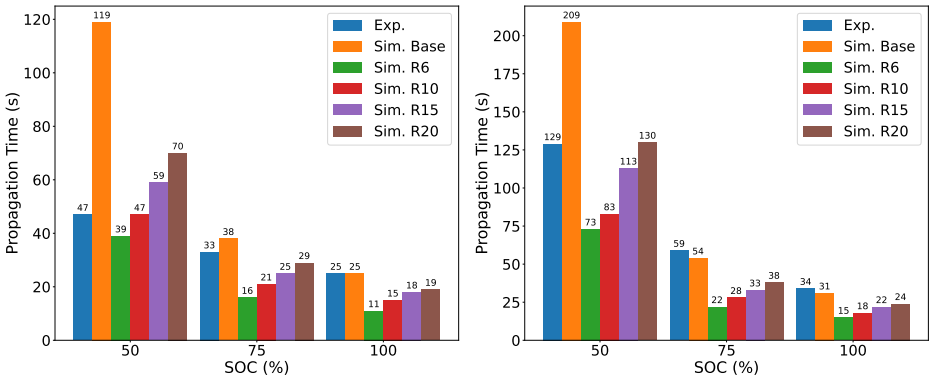

Figure 10: Propagation times of experiments (Exp.) and simulations (Sim.) for 10°C/min (left) and 50°C/min (right) post-processed from peak heating rate times.

4 Conclusion

Understanding propagation of thermal runaway at a range of conditions is critical for determining the hazards associated with systems of Li-ion batteries. This work focused on two relevant parameters, the battery SOC and external heating rate, through experiments and simulations of a module level thermal abuse scenario. Through experiments, it was shown that the SOC boundary between propagation and mitigation decreases as the heating rate decreases. The energy release versus SOC and relevant propagation times were also explored. In general, increasing SOC results in faster propagation and greater energy release due to the link between heat release and active material in the electrodes.

LIM1TR simulations of propagating thermal runaway with a range of particle sizes and BET surface areas were compared against experimental temperature measurements. While there is

substantial uncertainty in cell properties, predictions of propagation times and interface temperatures generally agreed at SOCs of 50% and greater for both heating rates studied. At the propagation/mitigation boundary, simulations erred on the side of mitigation and further efforts should be made to quantify the uncertainty in this boundary.

In summary, these experiments and simulations provide greater understanding of the cascading failure problem, and its sensitivity to SOC and heating rate. Future efforts should strive to integrate this knowledge in to system-scale thermal failure scenarios.

Acknowledgments

This work was funded by the U.S. Department of Energy, Office of Electricity, Energy Storage program. Dr. Imre Gyuk, Program Director. This article has been authored by an employee of National Technology & Engineering Solutions of Sandia, LLC under Contract No. DE-NA0003525 with the U.S. Department of Energy (DOE). The employee owns all right, title and interest in and to the article and is solely responsible for its contents. The United States Government retains and the publisher, by accepting the article for publication, acknowledges that the United States Government retains a non-exclusive, paid-up, irrevocable, world-wide license to publish or reproduce the published form of this article or allow others to do so, for United States Government purposes. The DOE will provide public access to these results of federally sponsored research in accordance with the DOE Public Access Plan https://www.energy.gov/downloads/doe-public-access-plan. This paper describes objective technical results and analysis. Any subjective views or opinions that might be expressed in the paper do not necessarily represent the views of the U.S. Department of Energy or the United States Government. SAND# SAND-XXXXX.

References

[1] P. Jindal, J. Bhattacharya, understanding the thermal runaway behavior of li-ion batteries through experimental techniques, Journal of The Electrochemical Society 166 (10) (2019) A2165.

[2] W.-C. Chen, Y.-W. Wang, C.-M. Shu, Adiabatic calorimetry test of the reaction kinetics and self-heating model for 18650 li-ion cells in various states of charge, Journal of Power Sources 318 (2016) 200–209.

[3] C.-Y. Jhu, Y.-W. Wang, C.-Y. Wen, C.-C. Chiang, C.-M. Shu, Self-reactive rating of thermal runaway hazards on 18650 lithium-ion batteries, Journal of thermal analysis and calorimetry 106 (1) (2011) 159–163.

[4] J. L. Lamb, L. Torres-Castro, J. C. Hewson, R. C. Shurtz, Y. Preger, Investigating the role of energy density in thermal runaway of lithium-ion batteries with accelerating rate calorimetry, J. Electrochem. Soc. 168 (6) (2021) 060516.

[5] A. O. Said, A. Garber, Y. Peng, S. I. Stoliarov, Experimental investigation of suppression of 18650 lithium ion cell array fires with water mist, Fire Technology 58 (1) (2022) 523–551.

[6] L. Torres-Castro, A. Kurzawski, J. C. Hewson, J. Lamb, Passive mitigation of cascading propagation in multi-cell lithium ion batteries, J. Electrochem. Soc. 167 (9) (2020) 090515.

[7] J. Kim, C. Yang, J. Lamb, A. Kurzawski, J. Hewson, L. Torres-Castro, A. Mallarapu, S. Santhanagopalan, A comprehensive numerical and experimental study for the passive thermal management in battery modules and packs, Journal of The Electrochemical Society 169 (11) (2022) 110543.

[8] A. Kurzawski, L. Torres-Castro, R. Shurtz, J. Lamb, J. C. Hewson, Predicting cell-to-cell failure propagation and limits of propagation in lithium-ion cell stacks, Proc. Combust. Instit. 38 (3) (2020) 4737–4745. doi:https://doi.org/10.1016/j.proci.2020.06.270.

[9] Z. Huang, T. Shen, K. Jin, J. Sun, Q. Wang, Heating power effect on the thermal runaway characteristics of large-format lithium ion battery with li (ni1/3co1/3mn1/3) o2 as cathode, Energy 239 (2022) 121885.

[10] C. Lee, A. O. Said, S. I. Stoliarov, Impact of state of charge and cell arrangement on thermal runaway propagation in lithium ion battery cell arrays, Transportation research record 2673 (8) (2019) 408–417.

[11] J. Fang, J. Cai, X. He, Experimental study on the vertical thermal runaway propagation in cylindrical lithium-ion batteries: Effects of spacing and state of charge, Applied Thermal Engineering 197 (2021) 117399.

[12] B. Ditch, D. Zeng, Fire hazard of lithium-ion battery energy storage systems: 1. module to rack-scale fire tests, Fire Technology (2020) 1–27.

[13] C. Jin, Y. Sun, H. Wang, Y. Zheng, S. Wang, X. Rui, C. Xu, X. Feng, H. Wang, M. Ouyang, Heating power and heating energy effect on the thermal runaway propagation characteristics of lithium-ion battery module: Experiments and modeling, Applied Energy 312 (2022) 118760.

[14] A. Kurzawski, R. Shurtz, Sand2021-12281, lim1tr: Lithium-ion modeling with 1-d thermal runaway v1.0, Report (October 2021).

[15] M. A. Hansen, J. C. Hewson, E. Armstrong, J. T. McConnell, J. C. Sutherland, R. C. Knaus, Spitfire v1.02.01 (2022).
URL `https://github.com/sandialabs/Spitfire`

[16] R. Shurtz, J. Engerer, J. Hewson, Predicting high-temperature decomposition of lithiated graphite: Part i. review of phenomena and a comprehensive model, J. Electrochem. Soc 165 (16) (2018) A3878–A3890.

[17] R. Shurtz, J. Engerer, J. Hewson, Predicting high-temperature decomposition of lithiated graphite: Part ii. passivation layer evolution and the role of surface area, J. Electrochem. Soc 165 (16) (2018) A3891–A3902.

[18] T. Hatchard, D. MacNeil, A. Basu, J. Dahn, Thermal model of cylindrical and prismatic lithium-ion cells, Journal of The Electrochemical Society 148 (7) (2001) A755–A761.

[19] M. Guo, G. Sikha, R. E. White, Single-particle model for a lithium-ion cell: Thermal behavior, Journal of The Electrochemical Society 158 (2) (2011) A122–A132.

[20] K. Zaghib, G. Nadeau, K. Kinoshita, Effect of graphite particle size on irreversible capacity loss, Journal of the Electrochemical Society 147 (6) (2000) 2110.

[21] E. Archibald, R. Kennedy, K. Marr, J. Jeevarajan, O. Ezekoye, Characterization of thermally induced runaway in pouch cells for propagation, Fire technology 56 (6) (2020) 2467–2490.

[22] D. A. Frank-Kamenetskii, Diffusion and Heat Transfer in Chemical Kinetics, Plenum Press, New York, 1969.

Figure captions